Inorganic Chemistry

ARTICLE

pubs.acs.org/IC

# Unraveling the Roles of the Acid Medium, Experimental Probes, and Terminal Oxidant, $(NH_4)_2[Ce(NO_3)_6]$, in the Study of a Homogeneous Water Oxidation Catalyst

Derek J. Wasylenko, Chelladurai Ganesamoorthy, Matthew A. Henderson, and Curtis P. Berlinguette*

Department of Chemistry and Institute for Sustainable Energy, Environment & Economy, University of Calgary, 2500 University Drive N.W., Calgary T2N-1N4, Canada

Supporting Information

**ABSTRACT:** The oxidation of water catalyzed by $[Ru(tpy)(bpy)(OH_2)](ClO_4)_2$ (**1**; tpy = 2,2′;6″,2″-terpyridine; bpy = 2,2′-bipyridine) is evaluated in different acidic media at variable oxidant concentrations. The observed rate of dioxygen evolution catalyzed by **1** is found to be highly dependent on pH and the identity of the acid; e.g., $d[O_2]/dt$ is progressively faster in $H_2SO_4$, $CF_3SO_3H$ (HOTf), $HClO_4$, and $HNO_3$, respectively. This trend does not track with thermodynamic driving force of the electron-transfer reactions between the terminal oxidant, $(NH_4)_2[Ce(NO_3)_6]$ (CAN), and Ru catalyst in each of the acids. The particularly high reactivity in $HNO_3$ is attributed to the $NO_3^-$ anion: (i) enabling relatively fast electron-transfer steps; (ii) participating in a base-assisted concerted atom-proton transfer process that circumvents the formation of high energy intermediates during the O−O bond formation process; and (iii) accelerating the liberation of dioxygen from the catalyst. Consequently, the position of the rate-determining step within the catalytic cycle can be affected by the acid medium. These factors collectively contribute to the position of the rate-determining step within the catalytic cycle being affected by the acid medium. This offering also outlines how other experimental issues (e.g., spontaneous decay of the Ce(IV) species in acidic media; CAN/catalyst molar ratio; types of catalytic probes) can affect the Ce(IV)-driven oxidation of water catalyzed by homogeneous molecular complexes.

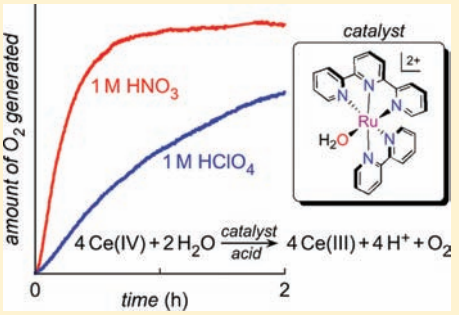


## INTRODUCTION

Experiments designed to characterize the performance of homogeneous water oxidation catalysts are often carried out in a strongly acidic medium using a sacrificial oxidant.[1−7] While this may provide the illusion of congruency in the field, there is actually significant variance in the experimental protocols used by different research programs (Supporting Information, Table S1). Catalytic reaction rate coefficients ($k_{cat}$), for instance, can be quantified by monitoring dioxygen evolution using various methods (e.g., Clarke electrode,[2,8−11] optical probe,[4,6,12] pressure transducer,[3,7,13,14] gas chromatography[15−17]), or monitoring the decay of the oxidant spectrophotometrically.[8,9,18−20] The majority of these studies use $(NH_4)_2[Ce^{IV}(NO_3)_6]$ (CAN) as the terminal oxidant (eq 1), but other chemical oxidants have also been employed (e.g., Co(III),[5] $[Ru^{III}(bpy)_3]^{3+}$[5,17,21−23] $OCl^-$,[10] and $HSO_5^-$[24]). Taking these disparities into account with the various solvent media used in each study imparts a general lack of clarity on how exactly reaction conditions affect catalytic performance.

$$4Ce(IV) + 2H_2O \xrightarrow{catalyst} 4Ce(III) + O_{2(g)} + 4H^+ \quad (1)$$

While a host of polymetallic[21,22,25−28] and bimetallic[5,10,15,29−37] complexes are capable of negotiating the multiple proton-coupled electron-transfer[38] (PCET) steps associated with the oxidation of water, the recent recognition that coordination complexes containing a single metal center can also oxidize water catalytically has heralded a significant advance for the field.[4,6,9,11,33,39−42] These systems are, in general, much easier to synthesize and study than multinuclear systems, and offer a robust platform for unraveling the intricate details of the catalytic cycle. This assessment prompted us to scrutinize the water oxidation catalyst, $[Ru(tpy)(bpy)(OH_2)]^{2+}$ (**1**; tpy = 2,2′;6″,2″-terpyridine; bpy = 2,2′-bipyridine; Scheme 1),[1,6,11] using a variety of probes and reaction conditions common to the field to better establish how experimental conditions affect the determination of catalytic parameters.

It has been shown that **1** adheres to an "acid-base" mechanism (black arrows in Scheme 1) that is closely aligned with the scheme documented by Meyer et al. for $[Ru(tpy)(bpm)(OH_2)]^{2+}$ (**2**; bpm = 2,2′-bipyrimidine).[9] The reactivity of **1**, however, is clearly influenced by the acid medium (Figure 1). While it has been noted that the pH can have an effect on the position of the rate-determining step (RDS),[43] it is not clearly established in the literature how acid conditions affect the behavior of water oxidation catalysts.[44,45] Indeed, it is not uncommon to compile a catalytic cycle where the reaction steps

**Received:** January 4, 2011
**Published:** March 17, 2011

have been measured in different acids. While this procedure is often difficult to avoid because of solubility issues, we show herein that this practice may not always depict the mechanism accurately (e.g., the position of the RDS may be affected by the acid medium). We offer clarity on these issues herein by unraveling how the acid medium can affect reactivity.

This report provides a comparative analysis of the Ce(IV)-driven oxidation of water catalyzed by **1** in four different acids [e.g., $HClO_4$, $CF_3SO_3H$ (HOTf), $HNO_3$, and $H_2SO_4$] at two different acid concentrations (i.e., 0.1 and 1.0 M) using two characterization methods common to the field, namely, a commercially available fluorescence optical probe and the spectrophotometric detection of Ce(IV) decay.[46,47] Given the divergent catalytic data observed in each of these acids, stopped-flow techniques were employed to examine the relative rates of select electron-transfer and O−O bond formation processes (i.e., $k_1$, $k_3$, and $k_{O-O}$) to better define each of the early reaction steps in Scheme 1. We also probe the dioxygen products formed over the course of the reaction using $^{18}O$-enriched water to examine the susceptibility of CAN to the undesirable auxiliary reaction pathway (defined as $k_{AUX}$ in Scheme 1) in each of the different acids. A compilation of the full suite of these results provides an important framework for characterizing homogeneous water oxidation catalysts.

## EXPERIMENTAL SECTION

**Preparation of Compounds.** Ligands and concentrated acid solutions were purchased from Aldrich, $RuCl_3 \cdot 3H_2O$ was purchased from Pressure Chemical Company; all reagents were used without further purification. Compound $[Ru(tpy)(bpy)(OH_2)](ClO_4)_2$ (**1**) was prepared and purified as previously reported.[6] HOTf acid solutions were prepared from reagent grade (>98%) HOTf as a 1.0 M solution in a glass bottle and stored over prolonged periods at 5 °C; the 1.0 M solution was sufficiently devoid of UV-absorbing impurities. $HClO_4$, $HNO_3$, and $H_2SO_4$ acid solutions were prepared from concentrated acid solutions and distilled, deionized water.

**Physical Methods.** Electrochemical measurements were recorded with a Princeton Applied Research VersaStat 3 potentiostat, a glassy carbon working electrode (diameter = 3 mm), a Pt wire counter electrode, and a [Ag]/[AgCl] reference electrode (3 M NaCl, 0.210 V vs NHE). Potentials reported herein are referenced to a normal hydrogen electrode (NHE). Electrochemical measurements of CAN in acid solutions (5 mL) were concluded within an hour of solution preparation with [CAN] = 31 mM.

Electronic spectroscopy data was collected on a Varian Cary 5000 UV−vis spectrophotometer. Kinetics measurements were performed by stopped-flow methods using a Hi-Tech Scientific SFA-20 coupled to the Cary 5000 spectrometer, and absorbance versus time traces were collected at appropriate wavelengths. Rate constants were determined by fitting absorbance versus time traces to a first- or second-order function using the kinetics fitting software supplied with the Varian Cary WinUV Kinetics Application software package (software version 3.00(182)) or manually using Microsoft Excel. Reported values of $k_1$ were collected by tracking the decay of the Ru(II) species (i.e., $(-d[Ru^{II}\text{-}OH_2]/dt = k_1[Ru^{II}\text{-}OH_2][CAN])$ under equimolar concentrations and repeated until standard deviations of ≤10% were achieved over at least five consecutive runs. At least three runs were carried out to determine $k_3$ and $k_{O-O}$ by tracking the absorbance signal versus time at 309 nm ($k_{O-O}$ could also be extracted by the signal at 688 nm). Unless specified otherwise, $k_3$ was determined by observing the spectral decay at 309 nm assigned as the decomposition of Ru(IV) or Ce(IV) (e.g., $(-d[Ru^{IV}{=}O]/dt = k_3[Ru^{IV}{=}O][CAN])$ species using the integrated rate law for a second order reaction, $1/[X]_t = 1/[X]_o - k_3t$ where [X] may represent either $[Ru^{IV}{=}O]^{2+}$ or [Ce(IV)] decay under equimolar conditions. $k_{O-O}$ was determined by fitting the onset of the spectral signature corresponding to the ostensible $[Ru^{III}\text{-}OOH]^{2+}$ species (i.e., $d[Ru^{III}\text{-}OOH]/dt = k_{O-O}[Ru^{III}\text{-}OOH]$) using the corresponding integrated rate law described by $\ln[(A - A_o)/(A_\infty - A_o)] = k_{O-O}t$, where $A$ = absorbance at time $t$; $A_o$ = absorbance at $t = 0$; $A_\infty$ = absorbance at $t_\infty$. Spectrophotometric experiments utilized the molar extinction coefficient ($\varepsilon$) value of the $\lambda_{max}$ associated with the MLCT band of **1** (476 nm; 9900 $M^{-1}$ $cm^{-1}$) for the accurate determination of [**1**]. Kinetic isotope effect (KIE) experiments were determined using the method of initial rates at roughly the same concentrations of catalyst and Ce(IV) in 0.1 M $HNO_3$ ($[Ru] = 3.8 \times 10^{-5}$ M; $[CAN] = 1.1 \times 10^{-3}$ M) and $HClO_4$ ($[Ru] = 3.9 \times 10^{-5}$ M; $[CAN] = 1.2 \times 10^{-3}$ M), but in $D_2O$ rather than $H_2O$; the KIE was measured spectrophotometrically by monitoring the decay of CAN at 360 nm and taking the relative ratios of reaction rates (i.e., $\{d[Ce(IV)]_H/dt\}/\{d[Ce(IV)]_D/dt\}$. In all of the above experiments, the CAN solutions were freshly prepared in the desired acid solutions and used within 5 min of preparation.

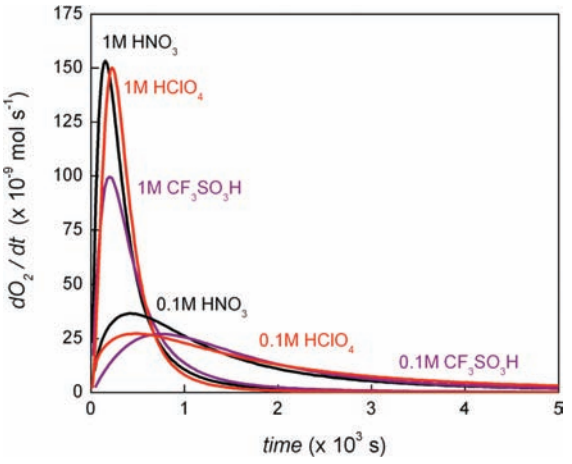


**Figure 1.** Acid dependence of the rate of dioxygen evolution as a function of time for the Ce(IV)-driven water oxidation reaction catalyzed by **1** ([CAN] = 0.11 M; [**1**] = $4 \times 10^{-4}$ M).

Dioxygen evolution was monitored using a custom-built apparatus consisting of a round-bottom flask equipped with a septum and a threaded side arm for insertion of the probe (working volume = 14.4 mL). The flask was charged with a solution of CAN in 3.0 mL of solvent, and the headspace was purged with $N_{2(g)}$ for about 20 min until a stable reading was obtained. Note the solution was not purged to ensure $O_2$ saturation and a rapid response for $O_2$ generated. A deaerated solution containing the catalyst was then injected through a rubber septum, and stirred in a temperature modulated oil bath (30 ± 2 °C) for the duration of the experiment. Dioxygen evolution was monitored every 10 s with an optical probe (Ocean Optics FOXY-OR125-AFMG) and a multifrequency phase fluorimeter (Ocean Optics MFPF-100). Data from the sensor was processed by the TauTheta Host Program and then converted into the appropriate calibrated $O_2$ sensor readings in "% $O_2$" by the OOISensors application. Standard deviation of the $O_2$ readings given by the instrument was determined to be ±3% of the total moles of $O_2$ produced from repeated control experiments, while standard deviations in the rates as obtained by this method were found to be ±10%. The $^{18}OH_2$ labeling studies were performed using water containing 9.87% $^{18}OH_2$ on a weight basis prepared from a 98.7% $^{18}OH_2$ solution purchased from Cambridge Isotopes Laboratories. Reactions were performed in the same apparatus as used for the dioxygen evolution studies. In a typical experiment, 2 mL of $^{18}OH_2$ (9.87%) was added to the flask followed by an appropriate amount of concentrated acid


dx.doi.org/10.1021/ic2000188 |Inorg. Chem. 2011, 50, 3662–3672

**Scheme 1. Proposed Reaction Pathways Describing Relevant (Proton-Coupled) Electron-Transfer Steps (e.g., $k_1-k_5$), O−O Bond Formation (e.g., $k_{O-O}$, $k_{AUX}$), and the Exclusion of Dioxygen (e.g., $k_{O2}$, $k_{O2}'$) during the Catalytic Oxidation of Water by 1 Driven by Ce(IV)[9,20,43,48] [a]**

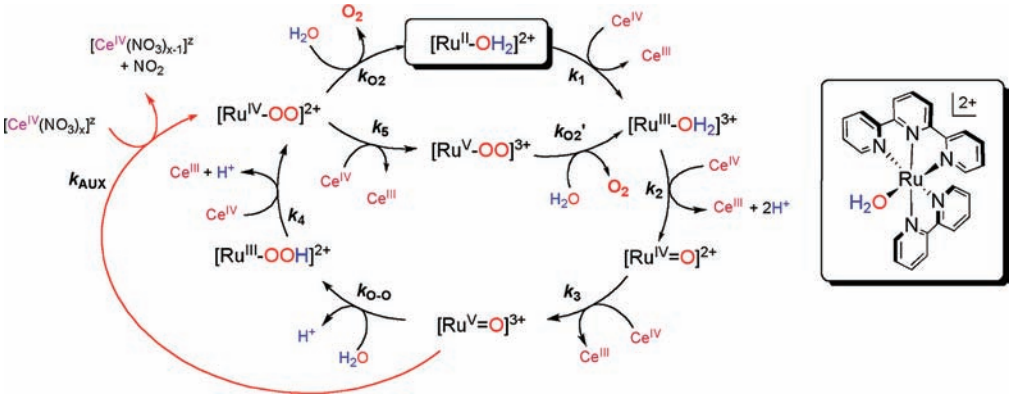


[a] Note that $k_{AUX}$ may also involve a free $NO_3^-$ anion rather than $[Ce(NO_3)_x]^z$.

solution (conc. $HNO_3$, 15.8 M; 70% $HClO_4$ 11.6 M) to achieve a 0.1 or 1.0 M acid concentration. For HOTf, an appropriate amount of triflic anhydride was added to achieve 0.1 and 1.0 M solutions. The flask was sealed after CAN was added to reach a concentration of 0.10 M; the solution and headspace were then purged with $N_{2(g)}$ until a stable dioxygen reading was obtained (ca. 20−30 min). A deaerated solution of the catalyst dissolved in $H_2O$ ($8.0 \times 10^{-7}$ mol) was then injected via syringe into the stirring CAN solution; the additional $^{16}OH_2$ content was taken into account. After the dioxygen reading had stabilized indicating the stoichiometric consumption of CAN, several 10−20 $\mu$L samples of the headspace were directly injected into a Varian 210GC/MS Ion Trap containing a Molsieve 5 Å gas separation column and an ion-trap set to focus on ions within the $m/z$ 20−80 range. Traces of individual ions were determined by extracting the desired $m/z$ value from the spectrum; relative concentrations of isotopes were determined by integrating the area under the signal of the appropriate extracted $m/z$ value. Introduction of atmospheric oxygen inherent to this method was corrected for by repeated injections of pure $N_2$ and noting the ratio of $O_2/N_2$, which was found to be 1.7 ± 0.4%. This ratio was then subtracted from the $^{32}O_2$ signal in the labeled $^{18}OH_2$ studies. All electrospray-ionization mass spectra (ESI-MS) were recorded on an Agilent Technologies 6520 Accurate-Mass Q-TOF LC/MS spectrometer. Instrument parameters were optimized to maximize observed spectra: capillary voltage (3200 V); source temperature (100 °C); desolvation temperature (300 °C); desolvation flow rate (250 L/h); cone voltage (20 V); collision voltage (1 V); quadrupole ion energy (2 V).

## RESULTS AND DISCUSSION

Following up on their pioneering work suggesting that a single Ru center is sufficient to oxidize water,[33] the Thummel group reported an extensive suite of single-site catalysts containing various polypyridyl ligands.[4] We have added to this library a series of compounds related to **1**, where the terminal substituents are varied while holding the local ligand environment at parity.[6] The results from our mechanistic studies show that **1**, in large part, conforms to the "acid-base" mechanism (denoted by black arrows in Scheme 1), first outlined by Meyer et al. for **2** and other single-site Ru catalysts.[9,48] The reaction sequence begins with two consecutive (proton-coupled) oxidation steps to furnish the $[Ru^{IV}{=}O]^{2+}$ species. A subsequent oxidation step generates the highly reactive $[Ru^{V}{=}O]^{3+}$ (or $Ru^{IV}$ oxyl) fragment, which is susceptible to nucleophilic attack by the incoming water substrate (i.e., $k_{O-O}$) to form $[Ru^{III}\text{-}OOH]^{2+}$.[9,48,49] A further proton-coupled electron-transfer (PCET) step leads to the formation of $[Ru^{IV}\text{-}OO]^{2+}$ (i.e., $k_4$), the species responsible for the exclusion of dioxygen in 0.1 M $HNO_3$ upon displacement by water (i.e., $k_{O2}$). Alternatively, the one-electron oxidation of $[Ru^{IV}\text{-}OO]^{2+}$ (i.e., $k_5$) occurs in 1.0 M $HNO_3$ prior to the loss of dioxygen to regenerate the $[Ru^{III}\text{-}OH_2]^{3+}$ species. The rate-determining step (RDS) at pH 1 was assigned as $k_{O2}$ (or $k_{O-O}$) within the "Ru(II)/Ru(V) cycle", while $k_5$ represents the RDS in the "Ru(III)/Ru(V) cycle" in 1 M $HNO_3$. We also identified an auxiliary (minor) reaction pathway, $k_{AUX}$, involving the abstraction of $O^{\bullet -}$ from a secondary oxygen source (e.g., $NO_3^-$, $[Ce(NO_3)_x]^z$).[20] A series of kinetic, isotopic labeling, ESI-MS experiments, and $NO_2$ evolution traces led us to conclude that a high-valent $[Ru{=}O]^z$ species is responsible for abstracting $O^{\bullet -}$ from $[Ce(NO_3)_x]^z$. This hypothesis is aligned with recent density functional theory (DFT) calculations by Sakai et al., showing radical character on a related Ce-nitrate salt, $[Ce(NO_3)_5OH]^{2-}$ (vide infra).[50]

Over the course of our experiments, a series of curious observations hinted at reaction conditions significantly affecting the reactivity of **1**. We therefore set out to examine the role of the acid medium on catalysis by tracking the Ce(IV)-driven oxidation of water in four different acids (e.g., $HClO_4$, HOTf, $HNO_3$, and $H_2SO_4$) at pH levels of 0 and 1. Catalytic activity was quantified by tracking dioxygen evolution in situ using an optical probe in the headspace of a closed reaction vessel to extract catalytic rates (defined as $k_{obs}$ herein), turnover numbers (TONs), and initial turnover frequencies (TOFs). The decay of the Ce(IV) salt under catalytic conditions was also quantified as a secondary means of establishing catalytic rate constants (defined herein as $k_{cat}$, where rate = $d[O_2]/dt = -d[Ce^{IV}]/4dt = k_{cat}[Ru]^n[CAN]^m$; $n$ and $m$ indicate orders of the reactants, and the coefficient takes into account that 4 equiv of Ce(IV) are required to generate one $O_2$ molecule) using a smaller concentration of CAN to avoid over-oxidation of the catalyst. The acid-dependence of select electron-transfer and O−O bond formation processes (i.e., $k_1$, $k_3$, and $k_{O-O}$) were determined to correlate the overall catalytic cycle to each of the principal reaction steps.

**Solution Behavior of the Terminal Oxidant, CAN.** We elected to use $(NH_4)_2[Ce(NO_3)_6]$ (CAN) as the terminal oxidant for this study because of its prevailing use in the field


dx.doi.org/10.1021/ic2000188 |Inorg. Chem. 2011, 50, 3662–3672

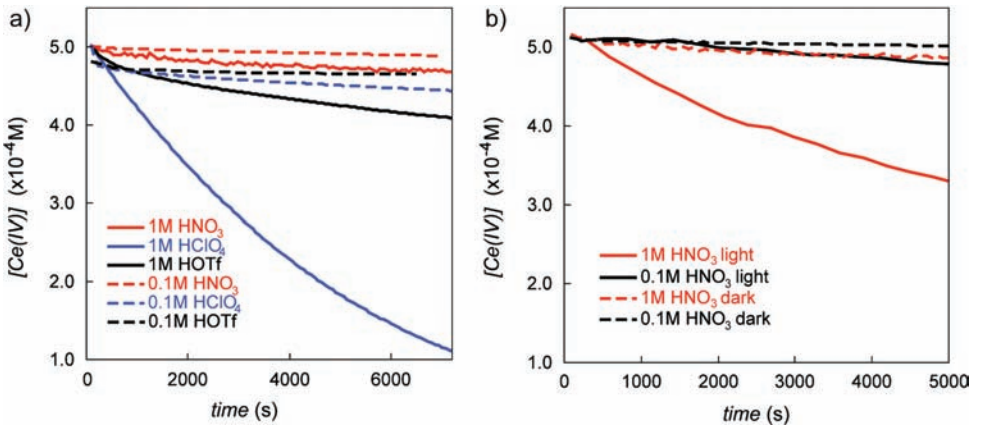


**Figure 2.** Time-dependent decay of CAN monitored at 360 nm in (a) $HNO_3$ (red), $HClO_4$ (blue), and HOTf (black) (data collected at 2-min intervals; samples stored in enclosed sample chamber over the course of the experiment); and (b) different concentrations of $HNO_3$ with (solid line) and without (dashed line) exposure to ambient laboratory light in between scans (data collected at 5-min intervals).

(Supporting Information, Table S1). It has been widely documented that CAN is a favorable one-electron transfer agent for these types of studies on the basis that it has a high oxidation potential ($E_{1/2}$ = +1.70 V vs NHE in 1.0 M $HClO_4$) with sluggish reactivity toward water in the absence of a catalyst,[51] it is unlikely to block any vacant coordination sites of the active catalyst, and has long been thought not to participate in any dioxygen formation pathways (although we[20] and Sakai et al.[50] have provided evidence to the contrary with respect to this latter point). We note that a potential limitation of CAN is that its utility is limited to pH ≤ 1 because of complications that arise from hydrolysis reations of Ce(IV) species, which, in turn, can go on to further react with the Ru catalyst.[50] While circumventing hydrolysis completely is unlikely, all catalytic studies herein were carried out in strongly acidic media to reduce the potential for delivery of an O moeity to the reactive $[Ru{=}O]^z$ unit.

Despite the rich history of cerate oxidimetry, the identities of the Ce(IV) species that exist *in solution* is not explicitly defined.[50,52−58] To provide further insight in this regard with respect to CAN, we recorded electrospray-ionization (ESI) mass spectra on a solution of CAN shortly after dissolution in 0.1 M solutions of HOTf, $HClO_4$, and $HNO_3$, and neat water (Supporting Information, Figures S1 and S2).[59] While we are cognizant that ESI-MS signal intensities do not necessarily reflect relative analyte concentrations,[60−65] the spectra nonetheless provide us with insight into what species are present in solution. The dominant Ce(IV) signal in the mass spectrum recorded in $HNO_3$ corresponds to $[Ce^{IV}(NO_3)_5]^-$ (Supporting Information, Figure S1). This species contrasts the solid-state structure of CAN being identified as $[Ce(NO_3)_6]^{2-}$;[66] however, we cannot rule out the possibility that a $NO_3^-$ ion is lost during the a charge-reduction process within the spectrophotometer. We also note evidence for some hydrolyzed species existing in solution, which may be responsible to some extent for the pH dependence of the electrochemical data (vide infra).[54,57,67] It has also been postulated that $[Ce(NO_3)_5OH]^{2-}$ is the species that interacts with the catalyst, where the $OH^{\bullet -}$ radical ligand undergoes O−O bond formation with the $[Ru{=}O]$ unit.[50] While we do not see evidence for $[Ce(NO_3)_5OH]^{2-}$ by ESI-MS, we do not dismiss the possibility that a pathway of this type is present. However, it does not account for the relative distribution of the O=O isotopomers in $HNO_3$ (vide infra) given that the hydroxide originates from water; thus, a pathway that involves abstraction of $O^{\bullet -}$ from a $NO_3^-$ ion is also needed (e.g., $k_{AUX}$).[20] Furthermore, the conditions used in the study by Sakai et al. were conducted in the absence of an acid buffer, which presumably enhances the concentration of the purported $Ce^{IV}/OH^-$ species in their proposal.

Dissolution of CAN in $HClO_4$ or HOTf renders a distribution of annated species with minor quantities of $[Ce^{IV}(NO_3)_5]^-$ still present in solution (Supporting Information, Figure S1 and Tables S2−S3). Recognition of this feature is important because the anions serve to shield the positive charge of the Ce(IV) ion from the cationic metal catalyst and will therefore affect intermolecular electron-transfer reactions. Furthermore, this interaction may affect the Ce(IV)/Ce(III) redox couple, which could have implications on catalysis (vide infra).

Our experiments revealed a disposition of the Ce(IV) salt absorbance spectrum to be affected upon light exposure under certain conditions, thereby prompting us to examine the rate of optical decay in each of the acids. (Note that the photolytic loss of $NO_3^{\bullet}$ from CAN in $HNO_3$ at 360 nm has been previously documented; eq 2.[68]) We monitored the absorbance signal of the Ce(IV) species as a function of time (Figure 2), which appears as a shoulder (i.e., $\lambda_{max}$ < 300 nm) in 0.1 M solutions of $HClO_4$, HOTf, and $HNO_3$. Data collection in 0.1 M $H_2SO_4$ was not successful because of precipitate formation [e.g., $Ce(SO_4)_2$]. The absorbance signal of $NO_3^-$ ($\lambda_{max}$ = 301 nm; ∼7.8 $M^{-1}$ $cm^{-1}$) also precluded spectrophotometric experiments from being carried out in 1.0 M $HNO_3$ that require monitoring at <350 nm. While there is minimal decay observed in HOTf and $H_2SO_4$ solutions, appreciable spectral decay occurs in $HClO_4$ and $HNO_3$ under ambient laboratory light (e.g., 60 W fluorescent light bulbs). This spectral decay is more prominent at higher molarities; e.g., 77% and 38% of the diagnostic signal is lost within 2 h in 1.0 M $HClO_4$ and $HNO_3$, respectively (Table 1; Figure 2). Although this process may be suppressed by preventing exposure to light (Figure 2b), these observations call attention to the importance of preparing fresh solutions of CAN prior to each catalytic run or stopped-flow experiment. Moreover, it also raises a potential issue with instruments (e.g., diode-array spectrometers) that expose the solution to broad spectral light for long time periods and/or ambient laboratory lighting.

$$[Ce^{IV}(NO_3)_x]^z \xrightarrow{h\nu} [Ce^{III}(NO_3)_{x-1}]^z + NO_3^{\bullet} \qquad (2)$$


dx.doi.org/10.1021/ic2000188 |*Inorg. Chem.* 2011, 50, 3662–3672

**Table 1. Summary of Experimental Parameters Relevant to the Study of the Catalytic Behavior of 1**

| | | | $(NH_4)_2[Ce(NO_3)_6]$ (CAN) | | | | $[Ru(tpy)(bpy)(OH_2)](ClO_4)_2$ (**1**)[e] | | |
|---|---|---|---|---|---|---|---|---|---|
| | | | | | relative decay[b,c] (%) | | $E^{o\prime}$ (V vs NHE) | | |
| acid | [acid] (M) | p$K_a$ | $E^{o\prime}$[a] (V vs NHE), Ce(IV)/Ce(III) | $\lambda_{max}$[b] (nm) | exposure to light[d] | no light exposure | Ru(III)/Ru(II) | Ru(IV)/Ru(III) | Ru(V)/Ru(IV)[f] |
| $HClO_4$ | 1 | −10 | 1.57 | 293 | 77 | 65 | 1.01 | 1.36 | 1.78 |
| | 0.1 | | 1.42 | 298, *s*[g] | 56 | 10 | 1.03 | 1.17 | 1.76 |
| HOTf | 1 | −14 | 1.53 | 289 | 16 | 15 | 1.02 | 1.30 | 1.71 |
| | 0.1 | | 1.41 | 295 | 12 | 3 | 1.04 | 1.14 | 1.76 |
| $HNO_3$ | 1 | −1.3 | 1.57 | <350[h] | 38 | 6 | 1.04 | 1.3[i] | 1.78 |
| | 0.1 | | 1.45 | 295, *s*[g] | 16 | 2 | 1.04 | 1.23 | 1.80 |
| $H_2SO_4$ | 1 | −3 | 1.53 | 318 | 3.3 | 2 | 1.03 | 1.3[i] | 1.70 |
| | 0.1 | | [j] | [j] | [j] | [j] | 1.04 | 1.15 | 1.70 |

[a] Values taken from cyclic voltammograms of a 31 mM solution of CAN in the respective acid solution at a scan rate of 50 mV/s. [b] [CAN] = 1.5−5.0 × $10^{-4}$ M. [c] Percent decay of diagnostic signal of CAN 90 min after dissolving the oxidant in the respective acid. [d] Ambient laboratory conditions illuminated by 60 W fluorescent light bulbs (no exposure to sunlight); Decay curves follow first order behavior: $k_{decay}$ = 2.6 × $10^{-4}$ $s^{-1}$ (1 M $HClO_4$), 9.5 × $10^{-5}$ $s^{-1}$ (0.1 M $HClO_4$), 1.5 × $10^{-5}$ $s^{-1}$ (1 M $CF_3SO_3H$), and 8.8 × $10^{-5}$ $s^{-1}$ (1 M $HNO_3$) when exposed to light. [e] [**1**] = 1 mM. [f] $E_{pa}$; observed with the onset of the catalytic wave. [g] *s* indicates shoulder. [h] Complete absorbance profile of Ce(IV) is masked by absorbance of $HNO_{3(aq)}$. [i] Poorly defined. [j] Value could not be obtained because Ce(IV) precipitates as $Ce(SO_4)_2$ in 0.1 M $H_2SO_4$.

Given that the acid medium appears to affect the identity of the Ce(IV) salt in solution, we examined the electrochemical behavior of CAN in each of the relevant acids. Each cyclic voltammogram (CV) was recorded using freshly polished glassy carbon electrodes (Supporting Information, Figure S3).[69] Electrochemical measurements of CAN at pH 0 were complicated by a very weak current response for the Ce(IV)/Ce(III) couple, and also the formal potential lying in the same region that solvent is oxidized at the glassy carbon electrode.[70] Consequently, square wave voltammetry was utilized to approximate the formal potential in each of the 1.0 M acid solutions.

An important outcome of these experiments is that data recorded at pH 1 discloses a relatively static Ce(IV)/Ce(III) formal potential in each of the acids (i.e., ∼1.45 V at pH 1; Table 1). While higher oxidation potentials were observed at pH 0, only a minor deviation in each of the different acids was observed (e.g., 1.53−1.57 V at pH 0; Table 1). Electrochemical experiments were performed on CAN in 0.1 M $HNO_3$ and $HClO_4$ solutions buffered with $KNO_3$ and $NaClO_4$, respectively, to render an ionic strength of 1.0 M. In both cases, the measured formal Ce(IV)/Ce(III) potential was found to be 1.43 V vs NHE, providing further evidence that the oxidizing capacity of CAN is pH dependent, but not necessarily acid dependent.[71] These observations are important because the purported sensitivity of the Ce(IV)/Ce(III) redox potential to acid type (e.g., +1.70 V in 1.0 M $HClO_4$; +1.61 V in 1.0 M $HNO_3$) is often used to rationalize relative rates of reactions for homogeneous water oxidation catalysts.[72] We, however, do not observe these differences using CAN, an inconsistency that arises because our data is recorded exclusively on CAN in the different acids; the formal oxidation potentials of CAN that are typically cited in the literature correspond to data recorded on other Ce(IV) salts.[51,53,70,73] We interpret this result to mean that the dissolution of CAN at pH 1 in HOTf and $HClO_4$ does not result in the full displacement of the $NO_3^-$ ligands from the Ce(IV) ion (supported by ESI-MS data at pH 1) and/or the different acid anions do not perturb electron density at the Ce(IV) ion to a significant extent. The pH dependence of the redox potentials (e.g., 150 mV/pH unit) does indicate that $[Ce(NO_3)_x]^z$ is doubly or triply protonated in solution. We do not, however, rule out the possibility of hydrolysis occurring to some extent even in acidic media, which is consistent with previous proposals put forth for CAN[50] and Pourbaix diagrams of $Ce(ClO_4)_2$.[56]

Cyclic voltammograms of CAN at pH 1 in each of the acids reveal peak potential differences ($\Delta E_p$) ranging from ∼0.08 V at slower scan rates ($\nu$ = 10−500 mV/s) to 0.20 V at $\nu$ = 1000−3000 mV/s. A linear relationship between peak current and $\nu^{1/2}$ between 10 and 250 mV/s was observed in each of the acids to confirm diffusion-controlled electron-transfer kinetics at the electrode surface. The ratios of anodic to cathodic peak currents ($i_{pa}/i_{pc}$), corrected for background current, reveal a clear acid dependence: $i_{p,a}/i_{p,c}$ = ∼1.6, ∼2.8, and ∼5.5 in 0.1 M solutions of HOTf, $HNO_3$, and $HClO_4$.[74] The observation that $i_{p,a}/i_{p,c}$ is >1 in each of the acids suggests that a chemical reaction involving the consumption of the Ce(IV) species (e.g., anion or solvent oxidation, photolysis) complements the heterogeneous redox event,[75] which may be related to the data in Figure 2 that shows instability of the Ce(IV) species in the different acid media.

**Physicochemical Properties of 1.** The next stage of this study was to define the physicochemical properties of **1** in each of the different acids (Table 1). The acid-dependence of the redox couples in each of the acids was not remarkable and will therefore be described only briefly here.[20] The CVs of **1** measured in each of the acids reveal two closely spaced reversible oxidation waves corresponding to metal-based Ru(III)/Ru(II) and Ru(IV)/Ru(III) redox processes. At both pH 0 and 1, the first oxidation step is solely an electron-transfer process, while the second oxidation process is accompanied with the loss of two protons (resulting in slow kinetics at the electrode and poor resolution) to form $[Ru^{IV}{=}O]^{2+}$ (Scheme 1; eqs 3 and 4).[20] In all cases, the onset of the Ru(V) wave ($E_{p,a}$ = 1.70−1.78 V) is concomitant with a catalytic wave corresponding to water oxidation (Supporting Information, Figure S4). CVs collected in $H_2SO_4$ reveal the presence of an additional cathodic wave at about +0.85 V ascribed to the


dx.doi.org/10.1021/ic2000188 |*Inorg. Chem.* 2011, 50, 3662–3672

**Table 2. Experimentally Determined (Proton-Coupled) Electron Transfer and Catalytic Rate Coefficients[a]**

| | | UV−vis | | | | optical probe | | |
|---|---|---|---|---|---|---|---|---|
| acid | [acid] (M) | $k_1$ ($\times 10^3$ $M^{-1}$ $s^{-1}$)[b] | $k_3$ ($M^{-1}$ $s^{-1}$)[d] | $k_{O-O}$ ($\times 10^{-4}$ $s^{-1}$)[g] | $k_{cat}$[i] | $k_{O2}$ ($\times 10^{-5}$ $s^{-1}$)[j] | initial TOF ($\times 10^{-3}$ $s^{-1}$) | eff.[k] (%) |
| $HClO_4$ | 1.0 | 280 | 200(20)[e] | *h* | 0.25 $M^{-1}$ $s^{-1}$ | 19 | 8.3 | ~100 |
| | 0.1 | 12 | 8(4)[e] | 1.2(3) | 5.0 × $10^{-5}$ $s^{-1}$ | 7.4 | 3.5 | 69 |
| $HNO_3$ | 1.0 | >600[c] | *f* | *h* | 8.8 $M^{-1}$ $s^{-1}$ | 93 | 46 | ~100 |
| | 0.1 | 44 | 4(1) | 2.3(1) | 1.6 × $10^{-4}$ $s^{-1}$ | 12 | 3.3 | 85 |
| HOTf | 1.0 | 110 | 90(30) | *h* | 0.13 $M^{-1}$ $s^{-1}$ | 8.9 | 5.0 | ~100 |
| | 0.1 | 21 | 3(1) | 1.2(3) | 4.0 × $10^{-5}$ $s^{-1}$ | 7.9 | 5.6 | 75 |

[a] [**1**] = 1−5 × $10^{-5}$ M. [b] Rate = $-d[Ru^{II}\text{-}OH_2]/dt = k_1[Ru^{II}\text{-}OH_2][CAN]$; measured by spectrophotometric monitoring of Ru(II) decay at 476 nm. [c] Faster than the time scale of the instrument, that is, $t_{1/2}$ < 0.033 s. [d] Rate = $-d[Ce^{IV}]/dt = k_3[Ru^{IV}{=}O][CAN]$; measured by spectrophotometric monitoring of Ce(IV) decay at 309 nm. [e] Reported value is likely inflated because of spontaneous Ce(IV) decay (see Figure 2). [f] Values cannot be determined because of absorbance by $NO_3^-$ (see text). [g] Rate = $d[Ru^{III}\text{-}OOH]/dt = k_{O-O}[Ru^{V}{=}O]$; measured by spectrophotometric monitoring of growth of the absorbance signal at 688 nm. Value in parentheses corresponds to standard deviation of ≥3 trials. [h] We did not find a spectroscopic signature at pH 0 that corresponds to $k_{O-O}$. [i] Rate = $-d[Ce^{IV}]/4dt = k_{cat}[Ru^{II}\text{-}OH_2][CAN]^n$, where *n* = 0 and 1 at pH 1 and pH 0, respectively. [j] Rate = $d[O_2]/dt = k_{O2}[Ru^{II}\text{-}OH_2]$; data is recorded under pseudo zero-order conditions in [CAN]; standard deviations are ±10%. [k] Efficiency (eff.) is defined as the number of moles of dioxygen produced per mole of oxidant present in the reaction flask: eff. = (mol $O_2$)/(mol CAN/4) × 100%, standard deviations are ±3%.

formation of an anated species, $[Ru(tpy)(bpy)(HSO_4)]^+$, generated at highly oxidizing potentials (Supporting Information, Figure S5).[5] The maximum of the signature metal-to-ligand charge-transfer (MLCT) band for **1** is centered at about 475 nm in all of the acids. Tracking the intensity of this band as a function of time revealed that **1** is stable over several hours in each the acid solutions except 1.0 M $HNO_3$, where it undergoes a spontaneous one-electron oxidation to form $[Ru^{III}\text{-}OH_2]^{3+}$.[76]

$$[Ru^{II}\text{-}OH_2]^{2+} + Ce(IV) \xrightarrow{k_1} [Ru^{III}\text{-}OH_2]^{3+} + Ce(III) \quad (3)$$

$$[Ru^{III}\text{-}OH_2]^{3+} + Ce(IV) \xrightarrow{k_2} [Ru^{IV}{=}O]^{2+} + Ce(III) + 2H^+ \quad (4)$$

**Acid-Dependence of Electron-Transfer and O−O Bond Formation Steps.** Stopped-flow spectrophotometric techniques were used to examine the acid-dependence of relevant bimetallic rates of electron-transfer between CAN and **1** in $HClO_4$, $HNO_3$, and HOTf (Table 2). The time-dependent decay of the Ru(II) signal was used to extract $k_1$, while $k_2$ was obtained by tracking the decay of CAN and/or the emergence of the shoulder of the $[Ru^{IV}{=}O]^{2+}$ species at 350 nm (Supporting Information, Figure S6). All $k_2$ values were found to be on the order of ~$10^3$ $M^{-1}$ $s^{-1}$; however, a further level of precision could not be certified and were therefore excluded from Table 2 to avoid providing a misleading portrayal of trends. The combination of equal concentrations of **1** and CAN follow second-order behavior (i.e., rate = $k$[**1**][CAN]) for bimetallic reaction steps $k_1$ and $k_2$. At pH 1, $k_1$ is slightly higher in $HNO_3$ than in $HClO_4$ and HOTf, which can, perhaps, be ascribed to the relatively higher thermodynamic driving force in $HNO_3$ (e.g., $\Delta G_{k1}$ = −40, −38, and −36 kJ $mol^{-1}$ in $HNO_3$, $HClO_4$, and HOTf, respectively).

The $k_1$ and $k_3$ electron-transfer steps are found to be faster at pH 0 than pH 1 by at least an order of magnitude, and the variability of these values in each of the different acids is significantly more pronounced at pH 0 than pH 1 (Table 2). Notably, $k_1$ is fastest in $HNO_3$ at both pH 0 and 1. On the basis of the thermodynamic data in Table 1, the $\Delta G_{rxn}$ values in each of the acids do not seem to account for the magnitude of $k_1$ in $HNO_3$ relative to $HClO_4$ and HOTf. Thus, it appears that the rate of electron-transfer between the Ce(IV) ion and the catalyst is dictated less by thermodynamic driving force than by kinetic factors, such as the $NO_3^-$ ion mediating faster electron-transfer between the two metal species.

Tracking the time-dependent absorbance trace of the $[Ru^{IV}{=}O]^{2+}$ form of the catalyst following the addition of 1 equivalent of CAN in each of the acids gives rise to some other intriguing observations. Meyer et al. have outlined how this procedure produces an initial decrease in absorbance at a relevant wavelength corresponding to the formation of the highly reactive $[Ru^{V}{=}O]^{3+}$ species (i.e., $k_3$), with a subsequent rise in optical response corresponding to the critical O−O bond formation step (i.e., $k_{O-O}$) to furnish the $[Ru^{III}\text{-}OOH]^{2+}$ complex.[9,18] Analogous behavior is observed for **1** in $HClO_4$ (Supporting Information, Figure S7) and HOTf at pH 1 (Figure 3). While we previously reported that tracking the optical response at 309 nm in 0.1 M $HNO_3$ does not reveal a signature consistent with a second reaction step,[77] a series of follow-up experiments have confirmed that there are indeed successive reaction steps. While we are unable to offer an explanation for this discrepancy, we now have the benefit of comparing both $k_3$ and $k_{O-O}$ in 0.1 M $HNO_3$ obtained by tracking the data at 309 nm (note that the onset at 688 nm corresponding to the putative $[Ru^{III}\text{-}OOH]^{2+}$ species also enables the extraction of $k_{O-O}$). (A viable spectroscopic signal corresponding to $k_{O-O}$ could not be determined at pH 0 in any of the acids because the derived rates were *slower* than $k_{cat}$.) The data recorded at pH 1 show that $k_{O-O}$ is approximately twice as fast in $HNO_3$ relative to the other acids. We attribute this result to the higher basicity of the $NO_3^-$ benefiting the O−O bond formation step in accordance with the base-assisted atom-proton transfer (APT) step documented by Meyer et al.[78] Within this scenario, the $NO_3^-$ acts as a base to accept a proton from the incoming $H_2O$ substrate during O−O bond formation to circumvent the formation of a higher energy intermediate (e.g., $[Ru^{III}\text{-}OOH_2]^{3+}$).[78] While a second water substrate can also act as a base (and is likely the case in HOTf and $HClO_4$), the reaction appears to be accelerated in $HNO_3$ because of the potentially higher basicity of $NO_3^-$; e.g., $H_3O^+$ and $HNO_3$ are characterized by (gas-phase) $pK_a$ values of −1.74 and −1.3, respectively.


dx.doi.org/10.1021/ic2000188 |*Inorg. Chem.* 2011, 50, 3662–3672

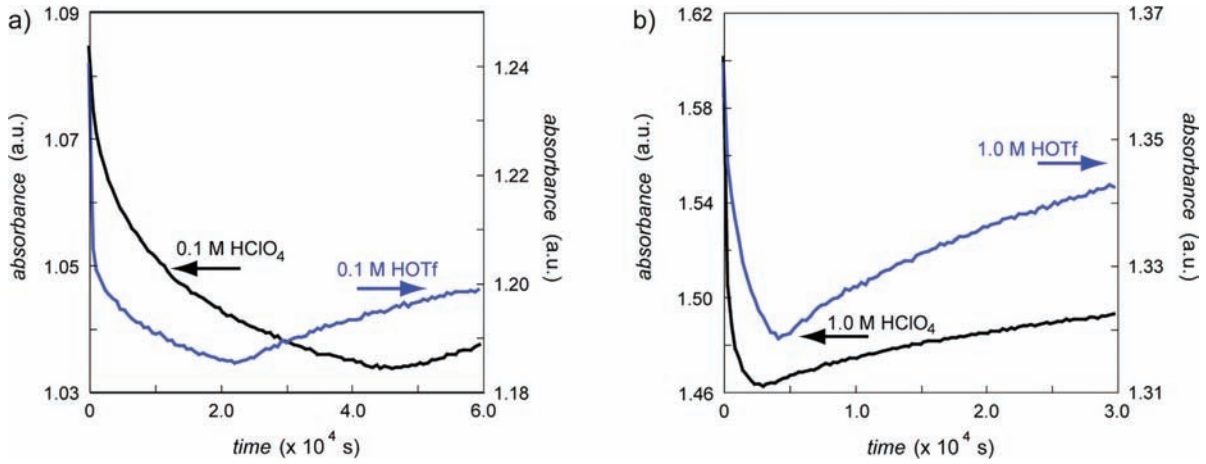


**Figure 3.** Time-dependent absorbance traces at $\lambda$ = 309 nm following the addition of 3 equiv of CAN to $[Ru^{II}\text{-}OH_2]^{2+}$ ([**1**] = 4.5−5.5 × $10^{-5}$ M) in $HClO_4$ and HOTf at (a) pH 1 and (b) pH 0. The absorbance changes are attributed to the successive reaction steps $k_3$ and $k_{O-O}$ (Scheme 1).

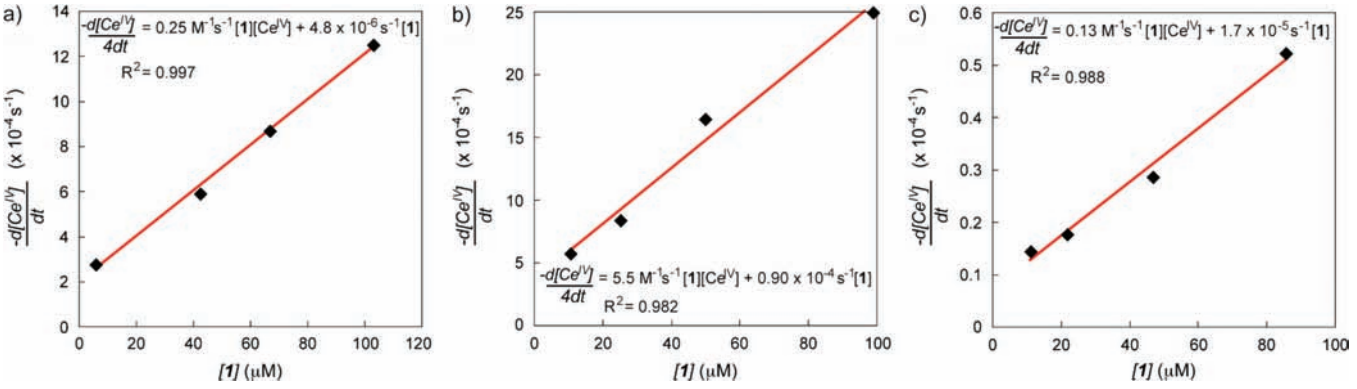


**Figure 4.** Spectrophotometric determination of $k_{cat}$ by monitoring the consumption of Ce(IV) at 360 nm using variable concentrations of **1** and 30 equiv of CAN in 1.0 M solutions of (a) $HClO_4$ ($\Delta t$ = 2000 s), (b) $HNO_3$ ($\Delta t$ = 500 s), and (c) HOTf ($\Delta t$ = 2000 s).

**Spectrophotometric Determination of $k_{cat}$.** The $k_{cat}$ values were obtained by monitoring the consumption of CAN at 360 nm spectrophotometrically under catalytic conditions (i.e., 30 equiv of CAN), and follow the same trends as $k_1$ in each of the acids (Table 2; Supporting Information, Figures S8 and S9). At pH 1, the reaction rate expression corresponds to $d[O_2]/dt = k_{cat}[\mathbf{1}]$ in each acid.[79] The RDS in $HNO_3$ is $k_{O-O}$ on the basis that it is resonant with $k_{cat}$ (i.e., ~2 × $10^{-4}$ $s^{-1}$). The RDS in HOTf and $HClO_4$ is assigned as $k_{O2}$ because $k_{cat}$ is first-order in [**1**] and slower than $k_{O-O}$. These observations indicate that $NO_3^-$ plays a role in enhancing the liberation of dioxygen because much faster catalytic rates are observed in $HNO_3$ and $k_{O-O}$ is the RDS; that is, $NO_3^-$ accelerates *both* $k_{O-O}$ and $k_{O2}$. In the other acids, the $k_{O2}$ step is significantly diminished and appears to become rate-limiting. (We do not rule out the possibility that $k_{O-O}$ can become rate-limiting in all acids under different reaction conditions given the slight differences in $k_{O-O}$ and $k_{cat}$ in this study.)

At pH 0, the rate expressions in each acid are better described as rate = $k_{cat}[\mathbf{1}][CAN]$, which are aligned with $k_5$ being the RDS. The slope of initial rates of Ce(IV) consumption versus [**1**] does not pass through the origin in any of the acids (Figure 4), thereby suggesting that the rate law expression contains another term that adds to the overall observed reaction rate. This second term likely contributes to the catalytic cycle in Scheme 1 (i.e., does not involve a deactivation pathway) because the catalyst efficiencies in each of the acids is found to be at least 100% (Table 2). On these grounds, we propose that $k_{O-O}$ (or possibly $k_{O2}$) is competitive with $k_5$, and the rate expression is more accurately described as $d[O_2]/dt = k_5[\mathbf{1}][CAN] + k_{O-O}[\mathbf{1}]$, where $k_5$ and $k_{O-O}$ are 5.5 $M^{-1}$ $s^{-1}$ and 9 × $10^{-5}$ $s^{-1}$, respectively, in 1.0 M $HNO_3$.

We note that spectrophotometric data in pure water revealed an absorbance trace at $\lambda$ < 400 nm that *increased* over time. This behavior is presumably a consequence of Ce(IV) hydroxides dominating reactivity;[50] thus, further experiments in the absence of acid buffer were not carried out in this study.

Analogous spectrophotometric experiments were carried out in 0.1 M $HNO_3$ and $HClO_4$ solutions at a constant ionic strength of 1.0 M using the aforementioned buffer conditions (Supporting Information, Figure S10; Table S4). The measured $k_{cat}$ value (0.48 $M^{-1}$ $s^{-1}$) in a 0.1 M $HNO_3$/0.9 M $KNO_3$ solution was not only much faster than data collected in a 0.1 M $HClO_4$/0.9 M $NaClO_4$ solution (0.053 $M^{-1}$ $s^{-1}$), but also faster than the values obtained in 1.0 M $HClO_4$ (0.25 $M^{-1}$ $s^{-1}$) and 1.0 M HOTf (0.13 $M^{-1}$ $s^{-1}$). Our interpretation of these results is that the higher ionic strength leads to $k_5$ being the RDS as a result of enhanced charge-transfer kinetics, which is aligned with the data obtained at pH 0.

**Kinetic Isotope Effect Experiments.** To further probe the identity of the RDS under catalytic conditions, experiments were conducted to study a possible H/D kinetic isotope effect (KIE) using deuterated 0.1 M $DNO_3$ and $DClO_4$ and comparing the


dx.doi.org/10.1021/ic2000188 |*Inorg. Chem.* 2011, 50, 3662–3672

relative values of the initial rates (i.e., KIE = $[d[Ce(IV)]_H/dt]/[d[Ce(IV)]_D/dt]$ of Ce(IV) consumption measured spectrophotometrically). The observed KIE in 0.1 M $DNO_3$ was determined to be 0.43, suggestive of an unsymmetrical transition state in the RDS that resembles the product (e.g., $[Ru^{III}\text{-}OOH_2]^{2+}$), or a preequilibrium step preceding the RDS. While our collective data is better aligned with the former scenario, studies are underway to verify this to be the case. This inverse KIE has been observed for organometallic Ir complexes under catalytic conditions;[80] however, the effect for **1** is more pronounced. In fact, the Ce(IV) decay trace was markedly nonlinear in 0.1 M $DNO_3$ indicative of a rate law that is nonzero-order in [CAN]. This data lends some credence to our assignment of the RDS in $HNO_3$ being $k_{O-O}$, and $NO_3^-$ (or CAN) participating in a base-assisted concerted APT step.[78] While free $NO_3^-$ may be sufficiently basic, an interaction with the Ce(IV) ion may further enhance the basicity of the $NO_3^-$ to benefit APT. In $HClO_4$, the $ClO_4^-$ anion is not basic enough to assist the APT process, thereby leading to a slower $k_{O-O}$ step. Our assignment of the RDS as $k_{O2}$ in $HClO_4$ is further supported by the lack of a KIE (i.e., KIE = 1.0) conducted in 0.1 M $DClO_4$. A correlation between $k_{cat}$ and acid p$K_a$ supports our proposal of how the acids affect the $k_{O-O}$ and $k_{O2}$ steps (Supporting Information, Figure S11).

**Catalytic Parameters Determined by Optical Probe.** Catalysis was also quantified by measuring dioxygen evolution in situ using a fluorescence optical probe in the headspace of a closed reaction vessel using a larger excess of CAN (i.e., CAN/**1** = 200:1). The amount of CAN is much greater than that used in the aforementioned spectrophotometric experiments in order to gain a sufficient signal-to-noise ratio for dioxygen detection. Over the course of our studies, we have found that at least 200 equiv of CAN is required to produce a satisfactory signal at catalyst concentrations appropriate for spectrophotometric experiments (i.e., $[\mathbf{1}] = 5 \times 10^{-5}$ M). This quantity of CAN saturates the absorbance signal in UV−vis experiments, which precludes a direct comparison of measurements obtained by the two techniques under *exactly* the same reaction conditions. This discrepancy is germane to our goal of delineating the role of the acid medium because six $NO_3^-$ anions comprise each molecule of CAN; that is, every experiment listed in Table 2 contains an appreciable amount of $NO_3^-$ regardless of the acid medium. The delivery of Ce(IV) as $(NH_4)_4Ce(SO_4)_4 \cdot 2H_2O$ was successful in certain acids, but the rate of dioxygen evolution was significantly lower because of anation of the catalyst, and/or the lower oxidizing potential of this salt (i.e., ~1.44 V vs NHE in 1 M $H_2SO_4$); the poor solubility of other Ce(IV) salts (e.g., $Ce(SO_4)_2$, $Ce(OH)_4$) precluded effective experiments completely devoid of $NO_3^-$.

The observed reaction rate coefficients for dioxygen evolution ($k_{obs}$) using this large excess of CAN generates pseudo first-order conditions in each of the acid solutions, which enables an exponential fitting of the time-dependent dioxygen evolution data (Table 2).[6,29] Representative fittings of dioxygen evolution collected in 1.0 M $HClO_4$ and $HNO_3$ are provided in Supporting Information, Figure S12. The *trends* in $k_{obs}$ values follow $k_{cat}$, including a markedly faster reaction rate in $HNO_3$. The absolute $k_{obs}$ values are, however, typically higher than $k_{cat}$ because of the higher amount of CAN used. The $k_{obs}$ values using an even larger excess of CAN (i.e., 5000 equiv) were all found to be on the same order of magnitude in the different acids (e.g., $3.6-5.8 \times 10^{-4}$ $s^{-1}$), with only a slight deviation in values at pH 0 and 1. This observation highlights how using a lower CAN/catalyst ratio can reveal more pronounced differences in reactivity. These conditions are also less likely to lead to issues such as over-oxidation and catalyst degradation.[44]

Using 200 equiv (rather than a much larger excess) of CAN also facilitates the extraction of a catalyst efficiency value. In 1.0 M acid solutions (except $H_2SO_4$), a stoichiometric amount of dioxygen evolution is observed (i.e., 100% catalyst efficiency); however, catalyst efficiency is diminished in all acids at pH 1. The lower values may be skewed to an extent by the spontaneous decomposition of Ce(IV) over the longer time frame of the experiment, but the deactivation of the catalyst cannot be ruled out under these conditions.[20] At higher concentrations of **1** (e.g., $4 \times 10^{-4}$ M), catalyst efficiency is about 100% at pH 0 and 1 because of the faster reactivity. The initial TOFs were also established with the optical probe by measuring the TONs over the first 30 min of the reaction. We provide this data because the TOFs may provide a more representative metric with respect to catalytic activity.[81] In the case of **1**, the TOFs for **1** follow similar trends to both $k_{cat}$ and $k_{obs}$ reflecting the stability of the complex.

**Isotopic Labeling Experiments.** To ascertain the origin of the oxygen in the gaseous product, we carried out a series of experiments using $^{18}O$-enriched water. A comparison of the ratios of the O═O isotopomers (i.e., $^{16}O{=}{}^{16}O$, $^{16}O{=}{}^{18}O$, $^{18}O{=}{}^{18}O$) observed in the gas phase reveal that there is an extrinsic source of oxygen for experiments carried out in $HNO_3$ (Table 3). Sources of oxygen other than water in the reaction flask include the $ClO_4^-$ counterions (2 equiv/**1**), free $NO_3^-$ derived from the acid (ca. 3000 equiv/**1** in 1.0 M $HNO_3$ and ca. 300 equiv/**1** in 0.1 M $HNO_3$), and CAN (1200 equiv/**1** for all acids). Given that our ESI-MS studies have shown that the high-valent forms of **1** may have a special affinity for $[Ce(NO_3)_5]^-$ over the other ions, we have postulated that $[Ce(NO_3)_x]^x$ is the source of adventitious oxygen, a claim that is corroborated by the evolution of $NO_2$ in the headspace of the flask under catalytic conditions.[20] O-atom exchange between water and $NO_3^-$ ions in $HNO_3$ was not observed on a time scale relevant to our studies, but we do note that it has been shown by McKenzie et al. to play an important role with catalysts of lower activities.[31] Interestingly, the $k_{AUX}$ pathway is suppressed in the other acids (Table 3). This observation can be rationalized by some of the $NO_3^-$ ligands about the Ce(IV) ion being displaced by the conjugate base of the acid medium. Experiments in HOTf, for example, will involve a Ce(IV) ion that is coordinated by $OTf^-$ ions, an anion that would be less susceptible to bond activation. Consequently, experiments in this acid medium appear to shunt the $k_{AUX}$ pathway and force reactivity through the acid−base mechanism. A similar result is observed in experiments carried out in $HClO_4$. These results lend some caution to carrying out water oxidation studies with CAN in $HNO_3$.

## SUMMARY

This article provides a comprehensive analysis of how reaction conditions can affect the evaluation of water oxidation catalysts that rely on CAN as the terminal oxidant. Complex **1** is a robust, well-defined catalyst that offers the rare opportunity to extract catalytic parameters in different media in the absence of substantial decomposition, annation, and solubility issues.[44] The critical message that this article delivers is that the acid medium can affect the reactivity of *both* the catalyst and the terminal oxidant, and therefore plays an integral role in measurements recorded under catalytic conditions. An examination of CAN in the different acids, for example, demonstrates that the salt


dx.doi.org/10.1021/ic2000188 |*Inorg. Chem.* 2011, 50, 3662–3672

**Table 3. Relative Abundance of $O_2$ Isotopomers Generated During the Oxidation of $^{18}OH_2$-Labeled Water by 1 at pH 1 and 0 Using Three Different Acid Anions[a]**

| | | relative abundance | | | | | |
|---|---|---|---|---|---|---|---|
| | | 0.1 M acids | | | 1.0 M acids | | |
| acid | ion | observed[b] | theoretical[c] | % deviation[d] | observed[b] | theoretical[c] | % deviation[d] |
| $HNO_3$ | $^{16}O=^{16}O$ | 0.90(4) | 0.84 | 7.9 | 0.97(1) | 0.85 | 14 |
| | $^{16}O=^{18}O$ | 0.092(34) | 0.16 | −41 | 0.031(7) | 0.15 | −79 |
| | $^{18}O=^{18}O$ | 0.0040(14) | 0.0072 | −44 | 0.0013(3) | 0.0063 | −79 |
| $HClO_4$ | $^{16}O=^{16}O$ | 0.82(1) | 0.84 | −2 | 0.85(1) | 0.85 | 0 |
| | $^{16}O=^{18}O$ | 0.17(1) | 0.15 | 10 | 0.15(1) | 0.15 | 0 |
| | $^{18}O=^{18}O$ | 0.0072(3) | 0.0071 | 0.4 | 0.0057(1) | 0.0063 | −10 |
| HOTf | $^{16}O=^{16}O$ | 0.823(2) | 0.837 | −1.7 | 0.86(2) | 0.86 | 1 |
| | $^{16}O=^{18}O$ | 0.170(1) | 0.156 | 9.3 | 0.14(2) | 0.14 | −4 |
| | $^{18}O=^{18}O$ | 0.0072(2) | 0.0072 | 0 | 0.0052(7) | 0.0059 | −11 |

[a] [**1**] = 2.9−3.4 × $10^{-4}$ M; [CAN] = 0.11 M; total volume acid =2.5−2.7 mL. [b] Values in parentheses represent one standard deviation of the measured values taken over at least three separate runs. [c] Probability of 10% $^{18}OH_2$-labeled water producing $^{32}O_2$, $^{34}O_2$, and $^{36}O_2$ is 0.81, 0.18, and 0.01, respectively; values in the table take dilution factors into account. [d] % deviation = (observed − theoretical)/theoretical ×100%; theoretical values assume both O atoms of dioxygen are derived from water.

spontaneously decomposes in acids with weakly coordinating anions, and is accelerated in the presence of ambient laboratory light conditions. This feature calls attention to the need to generate fresh solutions of CAN immediately prior to experiments. Moreover, the acid anion can provide access to pathways that may be competitive to dioxygen evolution in catalytic studies; for example, the acid anion can participate in the O−O bond formation step (i.e., $k_{AUX}$); spontaneous oxidation of **1** in 1 M $HNO_3$.[76] We note that the dependence of reaction conditions for catalysts that proceed through a different mechanism (e.g., radical coupling pathway[42]) was not investigated here.

The extent to which different experimental protocols affect reaction metrics has not been explicitly addressed to date, thereby rendering it difficult to reconcile the relative behavior of different catalysts in the literature. To help bridge this gap, we compared the catalytic rate coefficients using two independent methods (e.g., fluorescence optical probe, spectrophotometrically) using a wide range of CAN/catalyst ratios that are common to the field. Despite the different concentrations required for the two measurement techniques, the optical probe for dioxygen detection using a CAN/**1** ratio of 200:1 provides the same general trends in $d[O_2]/dt$ as those determined by tracking Ce(IV) decay spectrophotometrically with CAN/**1** ratio of 30:1 (Table 2). The slightly faster rates determined with the optical probe are attributed to the higher amount of CAN relative to **1**. A larger excess of CAN (i.e., ≫200 equiv of CAN/catalyst) leads to a convergence in catalytic parameters that may mask subtle mechanistic details.

The clear acid dependence of $k_{cat}$, $k_{obs}$ and the single reaction steps (e.g., $k_1$, $k_3$, $k_{O-O}$, $k_{O2}$) also has direct implications to developing mechanistic schemes akin to Scheme 1. For example, previous studies on the paradigmatic "blue dimer", $[(bpy)_2(H_2O)Ru^{III}ORu^{III}(OH_2)(bpy)_2]^{4+}$, have shown that higher reaction rates are observed in $HClO_4$ relative to the other acids. The variability in thermodynamic driving force is often invoked as the principal driver for this acid dependence on the basis that the Ce(IV) ion is cited to be a stronger oxidant in 1 M $HClO_4$ ($E^{o\prime}$, Ce(IV)/Ce(III) = 1.70 V) than 1 M $HNO_3$ ($E^{o\prime}$, Ce(IV)/Ce(III) = 1.61 V). While these trends are indeed consistent with the relative p$K_a$ values of the acids, our data contrasts these claims in two ways: (i) the formal oxidation potential of CAN is *not* sensitive to the acid medium when holding the pH at parity; and (ii) the highest $k_{obs}$ and $k_{cat}$ values are observed in $HNO_3$, not $HClO_4$. Our electrochemical analysis of CAN in each of the different acids is in better agreement with a previous report that the formal oxidation potential of CAN is not particularly sensitive to the acid medium.[82] (The notion that the Ce(IV)/Ce(III) potential is sensitive to the acid is likely rooted in comparing the redox data of Ce salts with more weakly coordinating anions.[51,53,70])

It is notable that reaction rates are much faster in $HNO_3$ than the other acids at the same pH. The $NO_3^-$ anion appears to not only mediate faster electron-transfer kinetics, but seems to enhance other steps in the catalytic cycle. The relatively high basicity of the $NO_3^-$ anion appears to play a critical role in accelerating reactivity by (i) assisting the rate-limiting O−O bond formation step via a concerted base-assisted APT process and (ii) enhancing the exclusion of dioxygen from the $[Ru^{IV}\text{-}OO]^{2+}$ species. While the O−O bond formation step is slower in the other acids, the liberation of dioxygen is significantly diminished and becomes rate-limiting in $HClO_4$ and HOTf. This finding is important because it shows that the position of the RDS in the catalytic cycle can be affected solely by the acid medium. This claim is corroborated by the disparate KIE data recorded in the different acids. While faster reactivity is observed in $HNO_3$, we caution that an O-atom derived from $NO_3^-$ may be incorporated into the final dioxygen product to a small extent via $k_{AUX}$. This auxiliary pathway can be suppressed in the other acids (Table 3), which is consistent with a study by Llobet et al. showing that the water oxidation catalyst, *cis*-$[Ru^{II}(bpy)_2(H_2O)_2]^{2+}$, proceeds through the acid−base mechanism exclusively in experiments conducted with CAN in 0.1 M HOTf.[7]

This study highlights the need to balance a number of experimental factors when extracting catalytic parameters for catalysts of this type. Our collective observations hint that water oxidation driven by CAN with catalysts related to **1**, for instance, may need to be carried out in HOTf to circumvent undesirable complications, for example, $k_{AUX}$ in $HNO_3$, spontaneous decay

of CAN in $HClO_4$, annation problems associated with $H_2SO_4$ and HCl. However, the slower reactivity of **1** in HOTf may lead to other drawbacks (e.g., lower catalytic TONs and efficiencies because of access to deactivation pathways) given that the higher redox levels of Ru catalysts are less stable; thus, the faster reactivity in $HNO_3$ can be advantageous despite the possibility of the $k_{AUX}$ pathway. The significant enhancement of catalytic activity in $HNO_3$ arising from a base-assisted APT process may also have implications in a practical setting.

## ■ ASSOCIATED CONTENT

**Supporting Information.** Additional experimental details are provided in Tables S1−S4 and Figures S1−S12. This material is available free of charge via the Internet at http://pubs.acs.org.

## ■ AUTHOR INFORMATION

**Corresponding Author**
*E-mail: cberling@ucalgary.ca.

## ■ ACKNOWLEDGMENT

We are grateful to the anonymous reviewers of this work for their constructive comments. This work was financially supported by the Canadian Natural Science and Engineering Research Council (NSERC), Canada Research Chairs, Canadian Foundation for Innovation, and Alberta Ingenuity.

## ■ REFERENCES

(1) Concepcion, J. J.; Tsai, M.-K.; Muckerman, J. T.; Meyer, T. J. *J. Am. Chem. Soc.* **2010**, *132*, 1545–1557.
(2) Yamada, H.; Siems, W. F.; Koike, T.; Hurst, J. K. *J. Am. Chem. Soc.* **2004**, *126*, 9786–9795.
(3) Bozoglian, F.; Romain, S.; Ertem, M. Z.; Todorova, T. K.; Sens, C.; Mola, J.; Rodriguez, M.; Romero, I.; Benet-Buchholz, J.; Fontrodona, X.; Cramer, C. J.; Gagliardi, L.; Llobet, A. *J. Am. Chem. Soc.* **2009**, *131*, 15176–15187.
(4) Tseng, H.; Zong, R.; Muckerman, J. T.; Thummel, R. *Inorg. Chem.* **2008**, *47*, 11763–11773.
(5) Rotzinger, F. P.; Munavalli, S.; Comte, P.; Hurst, J. K.; Grätzel, M.; Pern, F. J.; Frank, A. J. *J. Am. Chem. Soc.* **1987**, *109*, 6619–6626.
(6) Wasylenko, D. J.; Ganesamoorthy, C.; Koivisto, B. D.; Henderson, M. A.; Berlinguette, C. P. *Inorg. Chem.* **2010**, *49*, 2202–2209.
(7) Sala, X.; Ertem, M. Z.; Vigara, L.; Todorova, T. K.; Chen, W.; Rocha, R. C.; Aquilante, F.; Cramer, C. J.; Gagliardi, L.; Llobet, A. *Angew. Chem., Int. Ed.* **2010**, *49*, 7745–7747.
(8) Binstead, R. A.; Chronister, C. W.; Ni, J.; Hartshorn, C. M.; Meyer, T. J. *J. Am. Chem. Soc.* **2000**, *122*, 8464–8473.
(9) Concepcion, J. J.; Jurss, J. W.; Templeton, J. L.; Meyer, T. J. *J. Am. Chem. Soc.* **2008**, *130*, 16462–16463.
(10) Limburg, J.; Vrettos, J. S.; Liable-Sands, L. M.; Rheingold, A. L.; Crabtree, R. H.; Brudvig, G. W. *Science* **1999**, *283*, 1524–1527.
(11) Masaoka, S.; Sakai, K. *Chem. Lett.* **2009**, *38*, 182–183.
(12) Kanan, M. W.; Surendranath, Y.; Nocera, D. G. *Chem. Soc. Rev.* **2009**, *38*, 109–114.
(13) McDaniel, N. D.; Coughlin, F. J.; Tinker, L. L.; Bernhard, S. *J. Am. Chem. Soc.* **2008**, *130*, 210–217.
(14) Ellis, W. C.; McDaniel, N. D.; Bernhard, S.; Collins, T. J. *J. Am. Chem. Soc.* **2010**, *132*, 10990–10991.
(15) Sens, C.; Romero, I.; Rodriguez, M.; Llobet, A.; Parella, T.; Benet-Buchholz, J. *J. Am. Chem. Soc.* **2004**, *126*, 7798–7799.
(16) Nagoshi, K.; Yamashita, S.; Yagi, M.; Kaneko, M. *J. Mol. Catal. A: Chem.* **1999**, *144*, 71–76.
(17) Duan, L.; Xu, Y.; Zhang, P.; Wang, M.; Sun, L. *Inorg. Chem.* **2010**, *49*, 209–215.
(18) Concepcion, J. J.; Jurss, J. W.; Norris, M. R.; Chen, Z.; Templeton, J. L.; Meyer, T. J. *Inorg. Chem.* **2010**, *49*, 1277–1279.
(19) Duan, L.; Xu, Y.; Gorlov, M.; Tong, L.; Andersson, S.; Sun, L. *Chem.—Eur. J.* **2010**, *16*, 4659–4668.
(20) Wasylenko, D. J.; Henderson, M. A.; Ganesamoorthy, C.; Koivisto, B. D.; Osthoff, H. G.; Berlinguette, C. P. *J. Am. Chem. Soc.* **2010**, *132*, 16094–16106.
(21) Geletii, Y. V.; Huang, Z.; Hou, Y.; Musaev, D. G.; Lian, T.; Hill, C. L. *J. Am. Chem. Soc.* **2009**, *131*, 7522–7523.
(22) Yin, Q.; Tan, J. M.; Besson, C.; Geletii, Y. V.; Musaev, D. G.; Kuznetsov, A. E.; Luo, Z.; Hardcastle, K. I.; Hill, C. L. *Science* **2010**, *328*, 342–345.
(23) Cao, Y.; Bai, Y.; Yu, Q.; Cheng, Y.; Liu, S.; Shi, D.; Gao, F.; Wang, P. *J. Phys. Chem. C* **2009**, *113*, 6290–6297.
(24) Limburg, J.; Vrettos, J. S.; Chen, H.; de Paula, J. C.; Crabtree, R. H.; Brudvig, G. W. *J. Am. Chem. Soc.* **2001**, *123*, 423.
(25) Howells, A. R.; Sankarraj, A.; Shannon, C. *J. Am. Chem. Soc.* **2004**, *126*, 12258–12259.
(26) Sartorel, A.; Carraro, M.; Scorrano, G.; De Zorzi, R.; Geremia, S.; McDaniel, N. D.; Bernhard, S.; Bonchio, M. *J. Am. Chem. Soc.* **2008**, *130*, 5006–5007.
(27) Geletii, Y. V.; Botar, B.; Kögerler, P.; Hillesheim, D. A.; Musaev, D. G.; Hill, C. L. *Angew. Chem., Int. Ed.* **2008**, *47*, 3896–3899.
(28) Besson, C.; Huang, Z.; Geletii, Y. V.; Lense, S.; Hardcastle, K. I.; Musaev, D. G.; Lian, T.; Proust, A.; Hill, C. L. *Chem. Commun.* **2010**, *46*, 2784–2786.
(29) Xu, Y. H.; Akermark, T.; Gyollai, V.; Zou, D. P.; Eriksson, L.; Duan, L. L.; Zhang, R.; Akermark, B.; Sun, L. C. *Inorg. Chem.* **2009**, *48*, 2717–2719.
(30) Gao, Y.; Liu, J.; Wang, M.; Na, Y.; Akermark, B.; Sun, L. *Tetrahedron* **2007**, *63*, 1987–1994.
(31) Poulsen, A. K.; Rompel, A.; McKenzie, C. J. *Angew. Chem., Int. Ed.* **2005**, *44*, 6916.
(32) Wada, T.; Tsuge, K.; Tanaka, K. *Inorg. Chem.* **2001**, *40*, 329–337.
(33) Zong, R.; Thummel, R. *J. Am. Chem. Soc.* **2005**, *127*, 12802–12803.
(34) Gersten, S. W.; Samuels, G. J.; Meyer, T. J. *J. Am. Chem. Soc.* **1982**, *104*, 4029–4030.
(35) Naruta, Y.; Sasayama, M.; Sasaki, T. *Angew. Chem., Int. Ed.* **1994**, *33*, 1839–1841.
(36) Xu, Y.; Eilers, G.; Borgstrom, M.; Pan, J.; Abrahamsson, M.; Magnuson, A.; Lomoth, R.; Bergquist, J.; Polivka, T.; Sun, L.; Sundstrom, V.; Styring, S.; Hammarström, L.; Akermark, B. *Eur. J. Chem.* **2005**, *11*, 7305–7314.
(37) Wasylenko, D. J.; Ganesamoorthy, C.; Koivisto, B. D.; Berlinguette, C. P. *Eur. J. Inorg. Chem.* **2010**, 3135–3142.
(38) Huynh, M. H. V.; Meyer, T. J. *Chem. Rev.* **2007**, *107*, 5004–5064.
(39) Dau, H.; Limberg, C.; Reier, T.; Risch, M.; Roggan, S.; Strasser, P. *ChemCatChem* **2010**, *2*, 724–761.
(40) Savini, A.; Bellachioma, G.; Ciancaleoni, G.; Zuccaccia, C.; Zuccaccia, D.; Macchioni, A. *Chem. Commun.* **2010**, *46*, 9218–9219.
(41) Nyhlen, J.; Duan, L.; Akermark, B.; Sun, L.; Privalov, T. *Angew. Chem., Int. Ed.* **2010**, *49*, 1773–1777.
(42) Tong, L.; Duan, L.; Xu, Y.; Privalov, T.; Sun, L. *Angew. Chem., Int. Ed.* **2011**, *50*, 445−449.
(43) Chen, Z.; Concepcion, J. J.; Jurss, J. W.; Meyer, T. J. *J. Am. Chem. Soc.* **2009**, *131*, 15580–15581.
(44) Liu, F.; Concepcion, J. J.; Jurss, J. W.; Cardolaccia, T.; Templeton, J. L.; Meyer, T. J. *Inorg. Chem.* **2008**, *47*, 1727–1752.
(45) Hurst, J. K.; Cape, J. L.; Clark, A. E.; Das, S.; Qin, C. *Inorg. Chem.* **2008**, *47*, 1753–1764.
(46) Alstrum-Acevedo, J. H.; Brennaman, M. K.; Meyer, T. J. *Inorg. Chem.* **2005**, *44*, 6802–6827.

(47) A Clarke electrode has been proven by many research groups to be an effective tool for detecting dioxygen (see Supporting Information, Table S1). Unfortunately, our commercial device failed to yield an acceptable level of reproducibility and was therefore excluded from this study.
(48) Concepcion, J. J.; Jurss, J. W.; Brennaman, M. K.; Hoertz, P. G.; Patrocinio, A. O. T.; Murakami Iha, N. Y.; Templeton, J. L.; Meyer, T. J. *Acc. Chem. Res.* **2009**, *42*, 1954–1965.
(49) Wang, L.-P.; Wu, Q.; Van Voorhis, T. *Inorg. Chem.* **2010**, *49*, 4543–4553.
(50) Yoshida, M.; Masaoka, S.; Abe, J.; Sakai, K. *Chem.—Asian J.* **2010**, *5*, 2369–2378.
(51) Nair, V.; Deepthi, A. *Chem. Rev.* **2007**, *107*, 1862–1891.
(52) Heidt, L. J.; McMillan, A. F. *Science* **1953**, *117*, 75–76.
(53) Cotton, F. A.; Wilkinson, G.; Murillo, C. A.; Bochmann, M. *Advanced Inorganic Chemistry*, 6th ed.; John Wiley & Sons, Inc.: New York, 1999.
(54) Wadsworth, E.; Duke, F. R.; Goetz, C. A. *Anal. Chem.* **1957**, *29*, 1824–1825.
(55) Das, A. K. *Coord. Chem. Rev.* **2001**, *213*, 307–325.
(56) Yu, P.; O'Keefe, T. J. *J. Electrochem. Soc.* **2006**, *153*, C80–C85.
(57) Yu, P.; Hayes, S. A.; O'Keefe, T. J.; O'Keefe, M. J.; Stoffer, J. O. *J. Electrochem. Soc.* **2006**, *153*, C74–C79.
(58) Hayes, S. A.; Yu, P.; O'Keefe, T. J.; O'Keefe, M. J.; Stoffer, J. O. *J. Electrochem. Soc.* **2002**, *149*, C623–C630.
(59) Analogous experiments in 1.0 M acid solutions were not carried out to avoid having an adverse effect on the instrument.
(60) Moscato, B.; Landis, C. *Chem. Commun.* **2008**, 5785–5787.
(61) Di Marco, V. B.; Bombi, G. G. *Mass Spectrom. Rev.* **2006**, *25*, 347–379.
(62) di Lena, F.; Quintanilla, E.; Chen, P. *Chem. Commun.* **2005**, 5757–5759.
(63) Alfonso, I.; Astorga, C.; Gotor, V. *J. Inclusion Phenom. Macrocyclic Chem.* **2005**, *53*, 131–137.
(64) Wang, H.; Agnes, G. R. *Anal. Chem.* **1999**, *71*, 3785–3792.
(65) Wang, K.; Gokel, G. W. *J. Org. Chem.* **1996**, *61*, 4693–4697.
(66) Dvorkin, A. A.; Krasnova, N. F.; Simonov, Y. A.; Abashkin, V. M.; Yakshin, V. V.; Malinovskii, T. I. *Kristallografiya (Russ.)* **1984**, *29*, 471.
(67) Wadsworth, E.; Duke, F. R.; Goetz, C. A. *Anal. Chem.* **2002**, *29*, 1824–1825.
(68) Martin, T. W.; Glass, R. W. *J. Am. Chem. Soc.* **1970**, *92*, 5075–5083.
(69) Pt and Au electrodes were problematic for these experiments because of the onset of a catalytic current in water at the highly oxidizing potentials needed to identify the Ce(IV)/Ce(III) potential.
(70) Cofre, P.; Bishop, E. *Analyst* **1981**, *106*, 316–322.
(71) Other electrochemical parameters (e.g., $\Delta E_p$, $i_{p,a}/i_{p,c}$) were found to be very similar to those conducted in only the 0.1 M acid solution.
(72) Hirata, N.; Lagref, J. J.; Palomares, E. J.; Durrant, J. R.; Nazeeruddin, M. K.; Grätzel, M.; Di Censo, D. *Chem.—Eur. J.* **2004**, *10*, 595–602.
(73) Harris, D. C. *Quantitative Chemical Analysis*, 6th ed.; W. H. Freeman and Company: New York, 2004.
(74) $i_{p,a}/i_{p,c}$ ratios are constant over $\nu$ = 10−1000 mV/s in HOTf and $HNO_3$, but decrease from 5.5 at $\nu$ = 10 mV/s to 3.2 at $\nu$ = 1000 mV/s.
(75) Bard, A. J.; Faulkner, L. R. *Electrochemical Methods. Fundamentals and Applications*, 2nd ed.; John Wiley & Sons: New York, 2001.
(76) Moyer, B. A.; Meyer, T. J. *J. Am. Chem. Soc.* **1979**, *101* 1326–1328.
(77) This procedure could not be carried out in 1.0 M $HNO_3$ because the absorbance band associated with $NO_3^-$ at 301 nm (~7.8 $M^{-1}$ $cm^{-1}$) masks the absorbance features of interest at <350 nm.
(78) Chen, Z.; Concepcion, J. J.; Hu, X.; Yang, W.; Hoertz, P. G.; Meyer, T. J. *Proc. Natl. Acad. Sci. U.S.A.* **2010**, *107*, 7225–7229.
(79) The addition of >30 equiv of CAN to **1** results in a modest enhancement of reaction rates, an observation that suggests that the rate law cannot be strictly described as zero-order in CAN.
(80) Blakemore, J. D.; Schley, N. D.; Balcells, D.; Hull, J. F.; Olack, G. W.; Incarvito, C. D.; Eisenstein, O.; Brudvig, G. W.; Crabtree, R. H. *J. Am. Chem. Soc.* **2010**, *132*, 16017–16029.
(81) Catalyst degradation or other deactivation processes may skew the data away from expected first order behaviour over longer time periods, which is especially important for experiments carried out at pH 1.
(82) Wei, Y.; Fang, B.; Arai, T.; Kumagai, M. *J. Appl. Electrochem.* **2005**, *35*, 561–566.